Kinetic interpretation of resonance phenomena in low pressure capacitively coupled radio frequency plasmas

Sebastian Wilczek,[1] Jan Trieschmann,[1] Denis Eremin,[1] Ralf Peter Brinkmann,[1] Julian Schulze,[1,2] Edmund Schuengel,[2] Aranka Derzsi,[3] Ihor Korolov,[3] Peter Hartmann,[3] Zoltán Donkó,[3] and Thomas Mussenbrock[1]

[1]*Department of Electrical Engineering and Information Science, Ruhr University Bochum, Bochum, Germany*
[2]*Department of Physics, West Virginia University, Morgantown, West Virginia 26506, USA*
[3]*Institute for Solid State Physics and Optics, Wigner Research Centre for Physics, Hungarian Academy of Sciences, Konkoly Thege Miklós str. 29-33, 1121 Budapest, Hungary*

Low pressure capacitive radio frequency (RF) plasmas are often described by equivalent circuit models based on fluid approaches that predict the self-excitation of resonances, e.g., high frequency oscillations of the total current in asymmetric discharges, but do not provide a kinetic interpretation of these effects. In fact, they leave important questions open: How is current continuity ensured in the presence of energetic electron beams generated by the expanding sheaths that lead to a local enhancement of the conduction current propagating through the bulk? How do the beam electrons interact with cold bulk electrons? What is the kinetic origin of resonance phenomena? Based on kinetic simulations, we find that the energetic beam electrons interact with cold bulk electrons (modulated on a timescale of the inverse local electron plasma frequency) via a time dependent electric field outside the sheaths. This electric field is caused by the electron beam itself, which leaves behind a positive space charge, that attracts cold bulk electrons towards the expanding sheath. The resulting displacement current ensures current continuity by locally compensating the enhancement of the conduction current. The backflow of cold electrons and their interaction with the nonlinear plasma sheath cause the generation of multiple electron beams during one phase of sheath expansion and contribute to a strongly non-sinusoidal RF current. These kinetic mechanisms are the basis for a fundamental understanding of the electron power absorption dynamics and resonance phenomena in such plasmas, which are found to occur in discharges of different symmetries including perfectly symmetric plasmas. *Published by AIP Publishing.*
[http://dx.doi.org/10.1063/1.4953432]

I. INTRODUCTION

Low temperature capacitively coupled radio frequency (CCRF) plasmas are indispensable tools for etching and deposition processes in microelectronics production.[1–3] Due to their nonlinear nature and manifold complexity, they are challenging physical systems for theory and experiments. Driven by a strong demand for process optimization and control, there is a significant need for a detailed understanding of the complex particle power absorption dynamics on a nanosecond timescale within a radio frequency (RF) period, as well as the development of methods for their control.[4]

At low neutral gas pressures of a few Pa or less, CCRF discharges typically operate in a strongly non-local regime. In the so-called "α-mode," electron power gain occurs at sheath expansion[5] and due to electric field reversal during sheath collapse.[6–9] "Stochastic heating" was modeled extensively in the past on the basis of a hard wall assumption, as well as in terms of pressure heating.[10–20] During the phase of sheath expansion, beams of energetic electrons are generated and penetrate into the plasma bulk, where they sustain the discharge via ionization and may lead to non-Maxwellian (e.g., bi-Maxwellian) electron energy distribution functions (EEDF).[21–27] A variety of experimental results obtained by phase resolved optical emission spectroscopy (PROES)[22,23] as well as simulations[26,27] of single frequency capacitive discharges indicate an acceleration of a single electron beam during one sinusoidal sheath expansion.

Such discharges are often described by zero-dimensional global models based on fluid approaches (e.g., equivalent electrical circuits[28–30]) or spatially resolved models based on the cold plasma approximation[31] that predict the self-excitation of plasma series[29] and parallel[32–34] resonances. At low pressures, and predominantly in asymmetric discharges, these models predict the plasma series resonance (PSR) to be self-excited due to the non-linearity of the charge-voltage characteristic of the RF boundary sheaths and to strongly enhance the electron power absorption.[28–31,35–40] This leads to the presence of higher harmonics of the driving frequency in the total discharge current (i.e., a sinusoidal driving voltage can trigger the PSR accompanied by a strongly non-sinusoidal RF current). Experimentally, the harmonics of the RF current can be detected by different kinds of current sensors.[41–43] Based on PROES measurements, a temporal correlation between these high frequency modulations of the total current and the dynamics of energetic electrons was observed.[24]

Although many aspects of such resonance phenomena have been extensively investigated in the past, their kinetic interpretation is missing. In fact, most existing models leave important questions unanswered: How is current continuity ($\nabla \cdot \vec{j}_{\text{tot}} = 0$, where $\vec{j}_{\text{tot}} = \vec{j}_d + \vec{j}_c$ is composed of the displacement and conduction current density) ensured in the presence of beam electrons generated by the expanding boundary sheaths that lead to a local enhancement of the conduction current propagating through the bulk? How do these energetic beam electrons interact with cold bulk electrons and how do they affect the electron velocity distribution function (EVDF)? What is the kinetic origin of resonance phenomena? The answers to these important fundamental questions can only be provided by kinetic theory (e.g., Particle in Cell (PIC), hybrid models, or direct solutions of Boltzmann's equation) paired with the right set of diagnostics and interpretation. An important contribution in this context is the computational work of Vender and Boswell,[6] who used a kinetic simulation to demonstrate that the generation of an energetic electron beam during sheath expansion can trigger a beam-plasma instability that causes high frequency oscillations of the electron power absorption density adjacent to the expanding sheath edge. These computational predictions were later confirmed experimentally by O'Connell et al.[44,45] using PROES.

We go beyond a purely kinetic analysis by linking kinetic effects to resonance phenomena observed in the analysis of a non-sinusoidal total discharge current as well as its constituents and predicted by previous fluid based models. In this sense, we unify different theories and answer the above fundamental questions focused on the mutual links between both approaches. Based on Particle in Cell (PIC) simulations of a symmetric low pressure single frequency argon discharge, we demonstrate that energetic beam electrons accelerated by the expanding sheaths propagate into the plasma bulk. This propagation leads to significant charge densities which form a local electric field in the discharge center. Accordingly, cold bulk electrons are modulated on the timescale of the inverse local plasma frequency and move back to the expanding sheath. The nonlinear interaction of bulk electrons with the expanding sheath accelerates a second beam into the plasma bulk. This process is repeated until the sheath stops expanding and leads to the formation of multiple electron beams. Additionally, a local displacement current in the discharge center is present in order to compensate the local enhancement of the conduction current caused by the propagating beam electrons. We demonstrate that this is the kinetic nature of resonance effects in CCRF plasmas. It is based on local phenomena and generally occurs under any conditions in such low pressure plasmas.

This manuscript is structured as follows: The details of the PIC/Monte-Carlo collision (MCC) simulation are briefly described in Section II. The simulation results are presented and discussed in Section III, which is divided into three subsections, where the electron dynamics, their effects on the formation of particular shapes of the current waveforms, and a driving voltage amplitude variation are discussed, respectively. Finally, the results are summarized and conclusions are drawn in Section IV.

II. PARTICLE IN CELL SIMULATION WITH MONTE CARLO COLLISIONS

Our analysis is based on Particle-in-Cell/Monte-Carlo collisions (PIC/MCC) simulations.[46,47] This benchmarked code[48] resolves one spatial dimension perpendicular to the electrodes, and three dimensions in velocity space. The electrodes are assumed to be infinite, planar, parallel, and separated by a gap of length L. One of the electrodes (at $x = 0$) is driven by a sinusoidal voltage waveform, $\phi(t) = \phi_0 \sin(\omega_{\text{RF}} t)$, where $\omega_{\text{RF}} = 2\pi \cdot f_{\text{RF}}$, and the other electrode (at $x = L$) is grounded. In order to fulfill all stability conditions and to improve the spatio-temporal resolution, the number of numerical grid cells is set to 1024 and the number of time steps per RF cycle is chosen to be 4000. The number of super-particles is between 100 000 and 200 000 when convergence is achieved. A geometrically symmetric discharge is adopted to demonstrate that resonance phenomena are of general relevance even in relatively simple cases, where they are usually neglected. For most of this work, a driving voltage amplitude of $\phi_0 = 150$ V is adopted, but we also analyze the effect of changing the voltage amplitude to $\phi_0 = 300$ V. We use a driving frequency of $f_{\text{RF}} = 55$ MHz, an argon gas pressure of $p = 1.3$ Pa, and a relatively small electrode gap of $L = 1.5$ cm. Secondary electron emission and particle reflection at the electrodes are neglected in order to simplify the interpretation. The cross sections for electron-atom (excitation, ionization, and elastic) and ion-atom (isotropic and backward elastic scattering) collisions are taken from Refs. 49 and 50. This choice of input parameters (frequency, voltage, pressure, and gap) is made in order to ensure the presence of "strong" (in consideration of the symmetry) resonance effects, while keeping the analysis simple. A broad parameter variation is beyond the scope of this work, which focuses on a fundamental kinetic understanding of resonance phenomena. The underlying kinetic mechanisms are generally present in low pressure CCRF discharges under any discharge conditions.

III. RESULTS

Figure 1 shows the sinusoidal driving voltage waveform and the resulting total current density at the powered electrode obtained from the simulation as a function of time within one RF period at $\phi_0 = 150$ V. The current and the voltage are approximately 90° out of phase, and the total current is markedly non-sinusoidal, i.e., it contains a substantial amount of harmonics as a consequence of the self-excitation of the PSR.[22,28,31] This result shows that the self-excitation of the PSR is not restricted to asymmetric discharges such as assumed in a variety of fluid based models.

In the following, we will reveal the kinetic origin of resonance effects that lead to the generation of the non-sinusoidal total current as shown in Figure 1. In order to achieve this goal, we will first analyze the electron dynamics obtained from the simulation by focusing on characteristic reference times (t_1, t_2, t_3, t_4 marked in Figure 1) during the phase of sheath expansion at the powered electrode and by dividing the total electron population into different groups (i) according to their kinetic energies and (ii) their direction
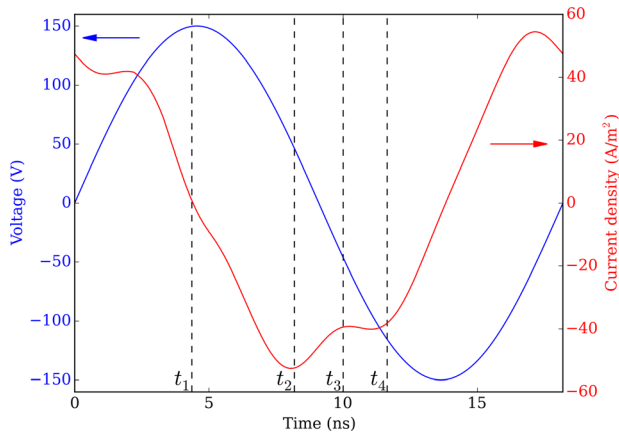
FIG. 1. Driving voltage waveform (left scale) and total current density at the powered electrode (right scale) obtained from the simulation as a function of time within one RF period. The vertical dashed lines indicate reference times (t_1, t_2, t_3, t_4) used in the forthcoming analysis. Discharge conditions: argon, 1.5 Pa, $L = 1.5$ cm, $f_{RF} = 55$ MHz, $\phi_0 = 150$ V.

of propagation along the discharge axis. Then, we will explain how these dynamics lead to the formation of distinct shapes of the waveforms of the conduction, displacement, and total current densities in the plasma. In this way, we provide a link between kinetic models and fluid interpretation. Finally, we study the effect of varying the driving voltage amplitude on the electron dynamics and the current waveforms.

A. Kinetic analysis of the electron dynamics

Under the conditions studied here, the motion of the argon ions is very weakly modulated, since $\omega_{pi} \ll \omega_{RF}$, where ω_{pi} is the ion plasma frequency. Thus, the ions follow the time-averaged electric field, and our analysis of the charged particle dynamics is restricted to the electrons.

Figure 2 shows spatio-temporal plots of the density of electrons split into different groups according to their kinetic energy ("hot"/"cold") as well as their direction of propagation along the discharge axis towards the powered or grounded electrode. The energy threshold for "hot" electrons is taken to be $\varepsilon_h = 11$ eV, close to the first excitation level of Ar atoms. "Cold" electrons are defined to have an energy below $\varepsilon_c = 4$ eV. The energy itself is calculated using all three velocity components $[\varepsilon_{h,c} = 0.5 m_e(v_x^2 + v_y^2 + v_z^2)]$. Here, the v_x-component (axial direction) is predominant, since it is much larger than the v_y and v_z components due to the fact that electrons are accelerated only in axial direction by the expanding sheaths and at the low pressure case considered here almost no collisions cause an angular scattering of electron beams. Electrons with $v_x > 0$ (i.e., those moving from the powered electrode towards the grounded electrode) are defined to move "upwards," while electrons with $v_x < 0$ are defined to move "downwards." Figure 2 includes vertical lines at the same characteristic times within one RF period as shown in Figure 1. The first row of Figure 2 shows spatio-temporal plots of the number densities of hot electrons moving upwards [Fig. 2(a)] and downwards [Fig. 2(b)]. The width of the sheath adjacent to the bottom (powered) electrode increases during the period when the driving voltage

waveform has a negative slope, from $t \approx 4.5$ ns to $t \approx 13.6$ ns, and decreases during the other half of the RF period, when the slope of the applied voltage is positive. The sheath at the top (grounded) electrode expands and contracts half an RF period shifted in time. Similarly to previous works,[22,36,51] the generation of multiple beams of energetic electrons is observed during one phase of sheath expansion. Here, two pronounced and one weak beam propagating upwards/downwards during the phase of sheath expansion at the powered/grounded electrodes are observed. Figures 2(c) and 2(d) show the corresponding density of cold electrons (moving up/downwards). The generation of multiple electron beams strongly affects the spatio-temporal ionization and excitation dynamics, which show similar structures[51] (i.e., this phenomenon is essential for the generation of such plasmas and is in contrast to classical assumptions of a single electron beam being generated per sheath expansion phase).

In the discussion to follow, the time-resolved electron velocity distribution function (EVDF) will be of great importance. In Figure 3, the EVDF is displayed as instantaneous snapshots at the marked characteristic times (spatially averaged over the plasma bulk; 6 mm $\leq x \leq$ 9 mm). In each plot, electrons with energies above 11 eV are represented by red bars, electrons with energies below 4 eV are marked in green, and electrons with energies between 4 eV and 11 eV are marked in blue. For reference, the dashed lines in Figure 3 correspond to a Maxwellian distribution fitted to the data shown in Figure 3(a).

The following discussion focuses on the phase of sheath expansion at the powered electrode. Due to the symmetry of the discharge, the same phenomena occur at the grounded electrode half an RF period later. During sheath collapse at the driven electrode ($t_1 \approx 4.4$ ns), the total current vanishes and the EVDF is approximately Maxwellian [Fig. 3: t_1]. After the sheath starts expanding at the powered electrode ($t_2 \approx 8.1$ ns), the first bunch of energetic beam electrons is generated and propagates towards the plasma bulk [Fig. 2(a)]. The number of these beam electrons is low compared with the number of cold bulk electrons, since the sheath expands in a region of low plasma density adjacent to the powered electrode at this time. As the sheath expands quickly, these beam electrons gain high velocities and propagate quickly through the bulk. This motion of the beam electrons away from the expanding sheath edge leads to a strongly anisotropic EVDF [Fig. 3: t_2], which deviates significantly from the initial Maxwellian (dashed). Clearly, the ensemble averaged electron energy, as well as the population of the high energy tail at positive velocities, are increased. As the energetic electrons of the first beam move away from the expanding sheath edge, they leave behind a positive space charge.

This can be observed in Figure 4 which shows the spatio-temporal evolution of the net charge density. A region of increased positive space charge (marked by a dashed rectangle) is found between t_2 and t_3 close to the sheath edge at about $x \approx 5$ mm. This positive space charge leads to the generation of a positive local electric field on the bulk side of the sheath edge during this time window that accelerates bulk electrons towards the powered electrode. Figure 5
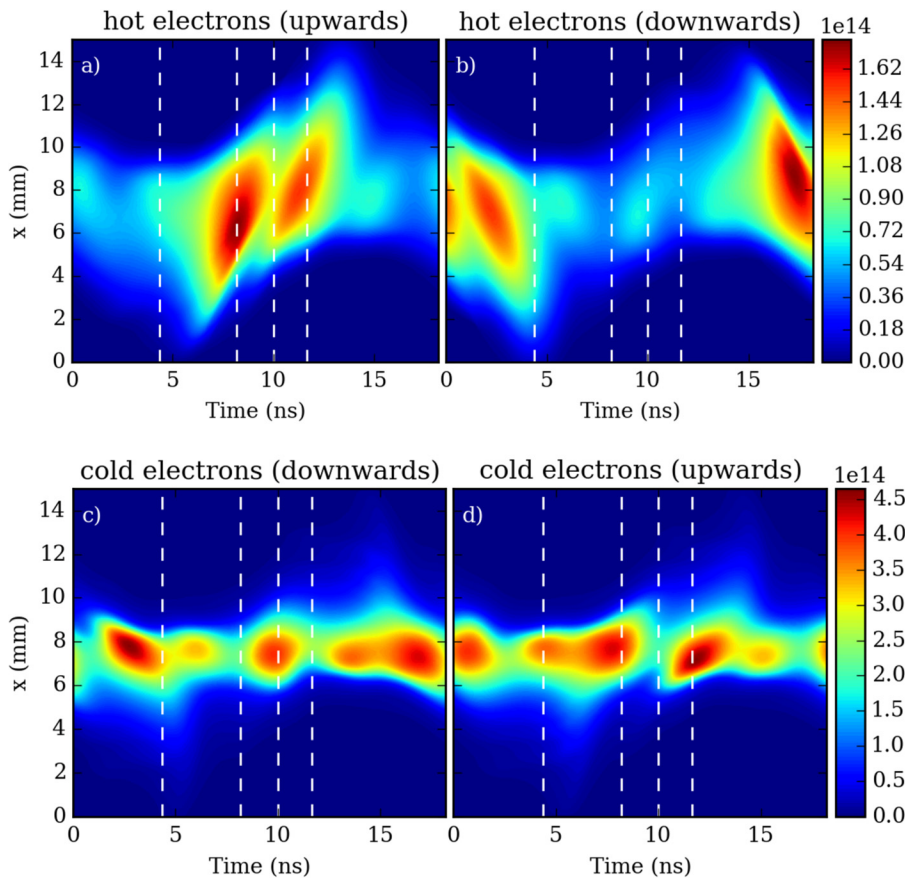
FIG. 2. Spatio-temporal plots of the density of "hot" electrons ($\varepsilon > 11\,\text{eV}$) that move upwards (a) and downwards (b) as well as the density of "cold" electrons below $4\,\text{eV}$ that move downwards (c) and upwards (d). The time axis covers one RF period. The densities are given in m^{-3}. The vertical dashed lines indicate the reference times specified in Figure 1. The powered electrode is located at $x = 0\,\text{mm}$, while the grounded electrode is located at $x = 15\,\text{mm}$. Discharge conditions: argon, $1.5\,\text{Pa}$, $L = 1.5\,\text{cm}$, $f_{RF} = 55\,\text{MHz}$, $\phi_0 = 150\,\text{V}$.
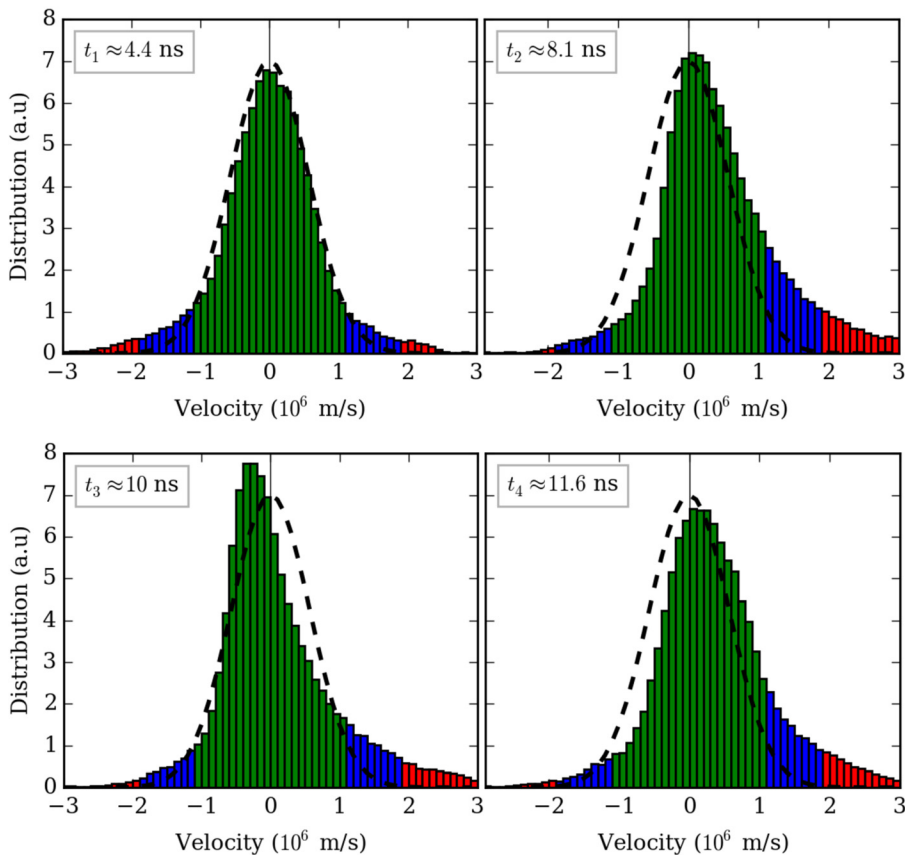
FIG. 3. Instantaneous electron velocity distribution function (EVDF) at the reference times, t_{1-4} marked in Figures 1 and 2, and spatially averaged over the plasma bulk ($6\,\text{mm} \leq x \leq 9\,\text{mm}$). The dashed lines indicate a Maxwellian fit generated at $t = t_1$. Electrons above $11\,\text{eV}$ are represented by red bars, electrons below $4\,\text{eV}$ by green bars, and electrons between 4 and $11\,\text{eV}$ by blue bars. Discharge conditions: argon, $1.5\,\text{Pa}$, $L = 1.5\,\text{cm}$, $f_{RF} = 55\,\text{MHz}$, $\phi_0 = 150\,\text{V}$.
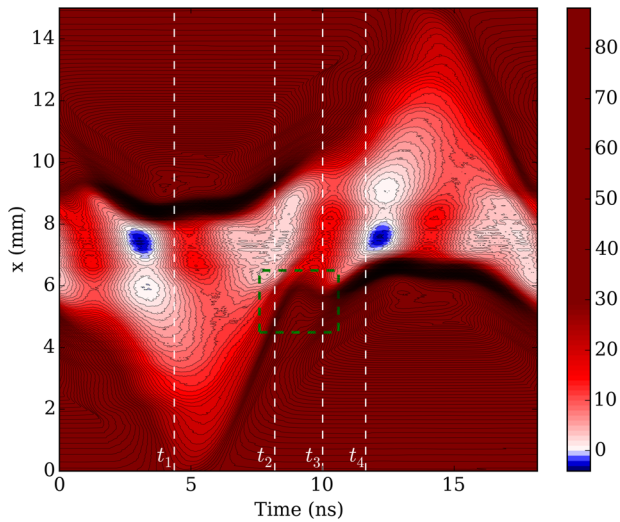
FIG. 4. Spatio-temporal distribution of the charge density in $\mu As/m^3$ within one RF period. The vertical dashed lines indicate the reference times specified in Figure 1. The green dashed rectangle indicates the non-sinusoidal dynamics of the region of positive space charge adjacent to the bottom plasma sheath. Discharge conditions: argon, 1.5 Pa, $L = 1.5$ cm, $f_{RF} = 55$ MHz, $\phi_0 = 150$ V.

FIG. 5. Spatio-temporal plot of the electric field in the entire discharge in V/m (left) and in the center of the discharge (right) as a function of time within one RF period. The vertical dashed lines indicate the reference times specified in Figure 1. Discharge conditions: argon, 1.5 Pa, $L = 1.5$ cm, $f_{RF} = 55$ MHz, $\phi_0 = 150$ V.

shows the electric field spatio-temporally resolved in the entire discharge (top) and in the discharge center as a function of time within one RF period (bottom), illustrating this effect. It is clearly shown that the electric field increases to a maximum between t_2 and t_3. As a consequence of this positive electric field and in order to compensate the positive space charge left behind by the beam electrons, shortly later (at $t_3 \approx 10$ ns) cold bulk electrons move towards the expanding sheath edge [Fig. 2(c)]. Therefore, at this time energetic beam electrons move upwards (represented mostly by the positive tail of the distribution), while cold bulk electrons move downwards. This is well observable in Figure 3(t_3), which shows two groups of electrons propagating into opposite directions simultaneously at this time. This is clearly a kinetic effect that cannot be described by a fluid model that is based on a mean velocity of the electrons. While the first electron beam propagates upwards through the plasma bulk, the cold bulk electrons ($n_{bulk} \approx 1.1 \times 10^{15}$ m^{-3}) cannot respond instantaneously to this perturbation, induced by the electron beam, due to their inertia. They can only respond on the timescale of the inverse local electron plasma frequency ($\omega_{pe} \approx 5\omega_{RF}$ in the bulk), which is approximately $\tau \approx 3.5$ ns ($\tau \approx 2\pi/\omega_{pe}$). This "delayed" reaction of the bulk electrons leads to the build up of the positive space charge on the bulk side of the sheath edge (Figure 4, green rectangle). In this region, the spatio-temporal distribution of the charge density indicates strongly non-sinusoidal dynamics between the sheath and the bulk, which leads to the local increase of the electric field around $t \approx t_2$ (Figure 5). This, in turn, is associated with a significant local displacement current, which is initially positive, when the positive space charge and the local electric field increase, and is later negative, when the cold bulk electrons compensate the positive space charge and the electric field decreases. These effects represent the kinetic origin why an "inductance" (i.e., electron inertia) is required in global equivalent circuit models to describe
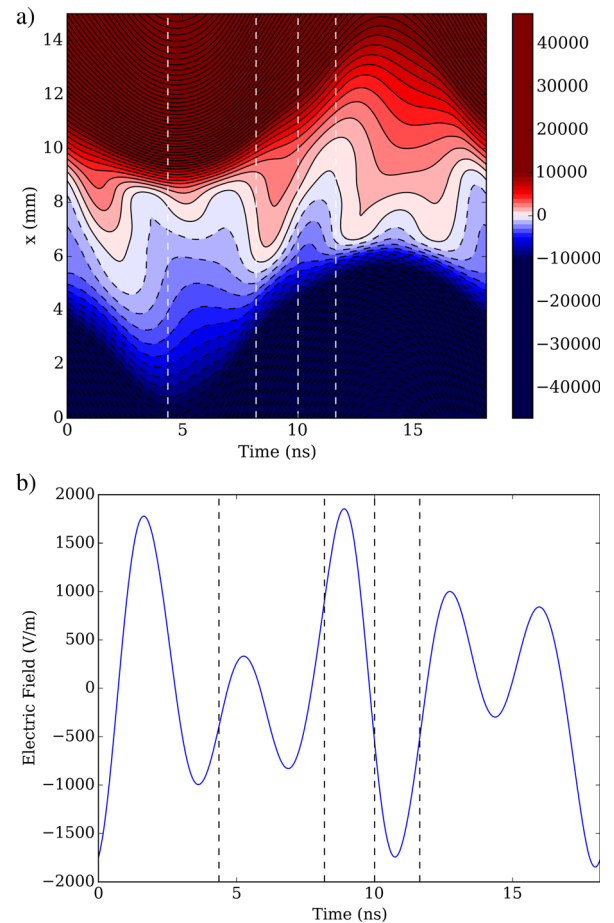
resonance effects. When the backflowing cold bulk electrons approach the moving potential barrier of the expanding sheath, the positive space charge is compensated and the electric field in the discharge center decreases to negative values. Due to their inertia, cold electrons continue to propagate towards the expanding sheath edge and upon impact a second beam of energetic electrons is generated [Figure 3 (t_4)]. This process is repeated throughout the phase of sheath expansion at the powered electrode. When the backflowing bulk electrons hit the expanding sheath, the sheath edge moves more slowly across a region of higher plasma density compared to the initial phase of sheath expansion, when the first beam was generated. Therefore, at $t \approx t_4$ a higher number of electrons is pushed towards the bulk at lower velocities and the formation of a negative space charge is observed in Figure 4 due to this compression of the electron system. Such a negative space charge is not observed, when the first electron beam is generated, since the beam electrons propagate into a region of positive space charge created by the last beam generated at the opposing electrode that propagates towards the powered electrode.

The number of electron beams per sheath expansion phase depends on the relation between the local response time of the electrons and the duration of sheath expansion.

Under these conditions, two pronounced energetic electron beams generated at the bottom powered electrode during one phase of sheath expansion can be observed at $t \approx 8.1$ ns and 11.6 ns. A third weak beam formation at 15 ns occurs close to the end of the expanding cycle, when the sheath expands very slowly.

The electron plasma frequency in the plasma bulk is about five times higher than the driving frequency of 55 MHz. Therefore, cold bulk electrons can move upwards/downwards 5 times per RF period in order to compensate positive space charges adjacent to the sheath edges caused by the propagation of energetic electron beams generated by the expanding boundary sheaths. This is confirmed by the presence of 5 maxima in Figures 2(c) and 2(d), respectively. This observation will play an important role in Sec. III B, when these kinetic effects will be linked to the dynamics of the conduction, displacement, and the total current to provide a kinetic interpretation of resonance effects.

B. Formation of current waveforms (displacement, conduction, and total current)

The previously discussed electron kinetics, including the interaction of hot beam electrons with cold bulk electrons via a local time dependent electric field generated by the electron beam itself, is the origin for the formation of the conduction, displacement, and total current waveforms at different positions within the discharge. Figure 6 shows spatio-temporal plots of the conduction and displacement current densities (the sum of which yields the total current density). Clearly, the propagation of energetic beam electrons causes a local enhancement of the conduction current that propagates through the plasma bulk (i.e., the conduction current density is strongly negative), when an electron beam propagates upwards to the grounded electrode, and strongly positive, when such a beam propagates downwards to the powered electrode. In fact, locally (in space and time) the conduction current density exceeds the total current density. This is illustrated in Figure 7 (left), which shows the total, conduction, and displacement current densities as a function of time in the discharge center.

At each time within the RF period current continuity (i.e., $\nabla \cdot \vec{j}_{tot} = 0$) must be fulfilled. This must also hold in the presence of a moving local enhancement of the conduction current density due to the propagation of energetic beam electrons. Current continuity is maintained via the local generation of a displacement current that instantaneously compensates the difference between the local conduction and the total current density (see Figures 6 and 7). Kinetically, this displacement current is a consequence of the generation ($\vec{j}_d > 0$ at t_2) and compensation ($\vec{j}_d < 0$ at t_3) of the positive space charge density caused by the propagating beam. These dynamics are shown in Figures 6 and 7. Once the cold bulk electrons move back towards the expanding sheath edge (at $t_3 \approx 10$ ns), the conduction current component caused by the energetic electron beam is compensated by the flux of cold bulk electrons into the opposite direction. Due to the electron inertia, this process produces an over-compensation such that the conduction current density reaches a local maximum at $t \approx t_3$ and again deviates from the total current density. This deviation is again compensated by the displacement current, which is now negative due to the decrease of the local electric field as a consequence of the compensation of the local positive space charge by the backflow of cold bulk electrons. In this way, current continuity is ensured at $t \approx t_3$. Finally, the backflowing cold bulk electrons hit the expanding sheath edge and the second beam is formed due to essentially the same mechanism. Once generated, it traverses through the bulk and creates a second minimum in the conduction current ($t_4 \approx 11.6$ ns) and the cycle repeats.

Further insights can be obtained from the Fourier amplitude spectra of the individual current density waveforms as shown in Figure 7 (right), for the center of the discharge. For the total current (time-varying, but constant along the discharge gap), the amplitude of the third harmonic is approximately 10.6% and the fifth harmonic is 7.5% of that of the fundamental frequency. The seventh and higher harmonics are negligibly small (less than 1%). Even harmonics are not excited due to the symmetry of the discharge.[52] Considering the conduction and displacement current densities, the observed harmonics (except for the fundamental) are 180° out of phase. Their amplitudes are determined by the criterion of total current continuity everywhere and at all times. In perspective of the local plasma parallel resonance (PPR), which was investigated by Ku *et al.*,[32–34] this compensation occurs at every location (infinitesimal LC-circuit element in an equivalent circuit model) when the local conduction current density—triggered by the beam electrons—exceeds the local total current density. Thus, a significant PPR is present under these conditions. The higher harmonics of the
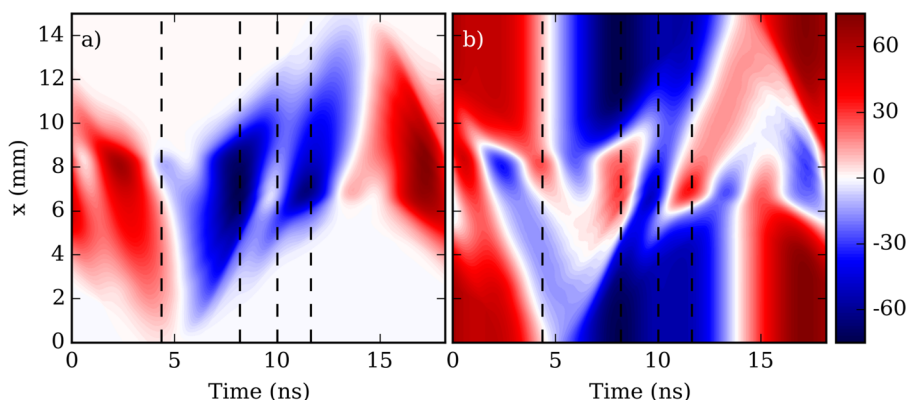
FIG. 6. Spatio-temporal plots of the conduction (a) and displacement (b) current density within one RF period in A/m². The vertical dashed lines indicate the reference times specified in Figure 1. Discharge conditions: argon, 1.5 Pa, $L = 1.5$ cm, $f_{RF} = 55$ MHz, $\phi_0 = 150$ V.
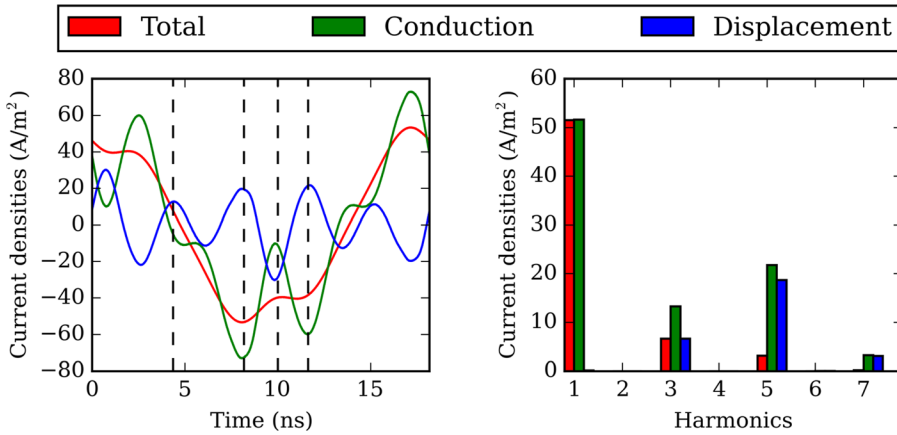
FIG. 7. Total, conduction, and displacement current densities in the discharge center at 7.5 mm as a function of time within one RF period (left) and their corresponding Fourier spectra (right). Discharge conditions: argon, 1.5 Pa, $L = 1.5$ cm, $f_{RF} = 55$ MHz, $\phi_0 = 150$ V.

conduction and displacement current densities do not compensate each other completely so that a significant dissipative higher harmonics component of the total current remains. This corresponds to the self-excitation of the PSR, which leads to Non-Linear Electron Resonance Heating (NERH).

In conclusion, both the PPR and the PSR are present and were explained at the kinetic level, based on the interaction between energetic beam electrons accelerated by the expanding sheaths and cold bulk electrons via a local time dependent electric field generated by the electron beam itself due to a positive space charge left behind by the propagating beam. These kinetic effects and, therefore, also the PPR and the PSR are different at each axial position. Thus, a complete understanding of such resonance phenomena requires a spatially resolved local and kinetic analysis of the electron dynamics.

C. Voltage variation

A variation of different external control parameters (gas pressure, geometry of the discharge, driving frequency, and voltage) has a significant influence on the spatio-temporal electron dynamics and the self-excitation of resonance effects. An important factor in this respect is the local plasma density, which determines the local electron plasma frequency. This in turn determines the reaction time of bulk electrons to the beam perturbations and, therefore, the number of energetic electron beams generated per sheath expansion phase at a given electrode. In the following, we investigate the effect of increasing the driving voltage amplitude from 150 V to 300 V.

Figure 8 shows the spatio-temporal distributions of "hot" electrons ($\varepsilon > 11$ eV) moving upwards (a) and "cold" electrons ($\varepsilon < 4$ eV) moving downwards (b) for $\phi_0 = 300$ V. Increasing the driving voltage amplitude to 300 V leads to more ionization and, therefore, an increased bulk electron density of $n_{bulk} \approx 3.4 \times 10^{15}$ m^{-3} and a higher electron plasma frequency of $\omega_{pe} \approx 9\omega_{RF}$ in the bulk. Thus, in comparison with the previously discussed case ($\phi_0 = 150$ V), the bulk electrons can respond faster to the perturbations caused by energetic electron beams generated by the expanding sheaths. The characteristic time-scale of the local backflow of cold bulk electrons towards the expanding sheath edge is

reduced to $\tau \approx 2$ ns. Therefore, for the fixed duration of the sheath expansion phase (determined by the driving frequency), the above described cyclic process is repeated more often during one phase of sheath expansion (i.e., an energetic electron beam is generated by sheath expansion leaving behind a positive space charge, which is compensated by a delayed backflow of cold bulk electrons, which upon impact at the expanding sheath leads to the generation of the next
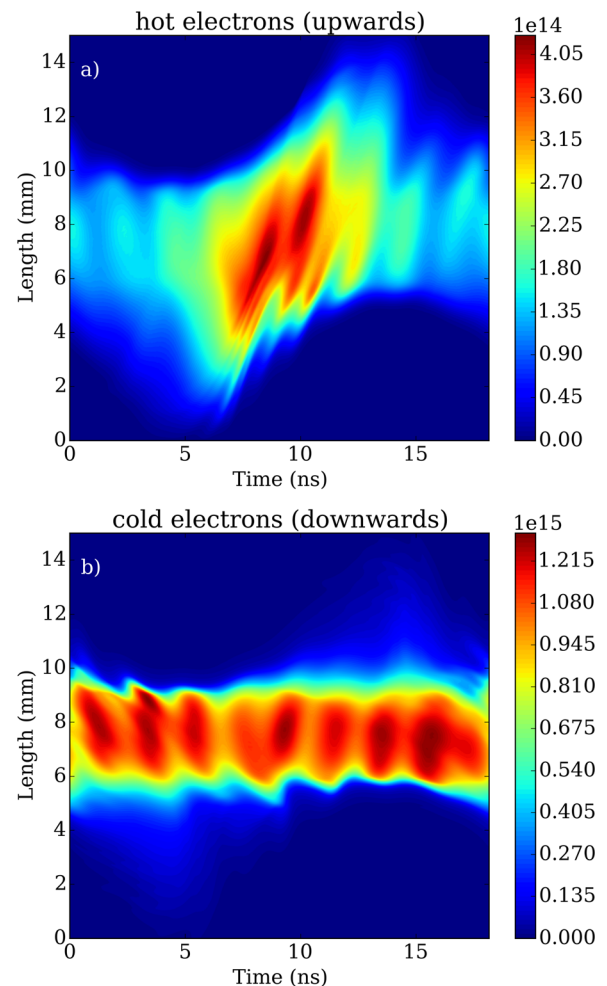
FIG. 8. Spatio-temporal plot of the density of "hot" electrons ($\varepsilon > 11$ eV) that move upwards (a) and of the density of "cold" electrons below 4 eV that move downwards (b) in m^{-3}. Discharge conditions: argon, 1.5 Pa, $L = 1.5$ cm, $f_{RF} = 55$ MHz, $\phi_0 = 300$ V.
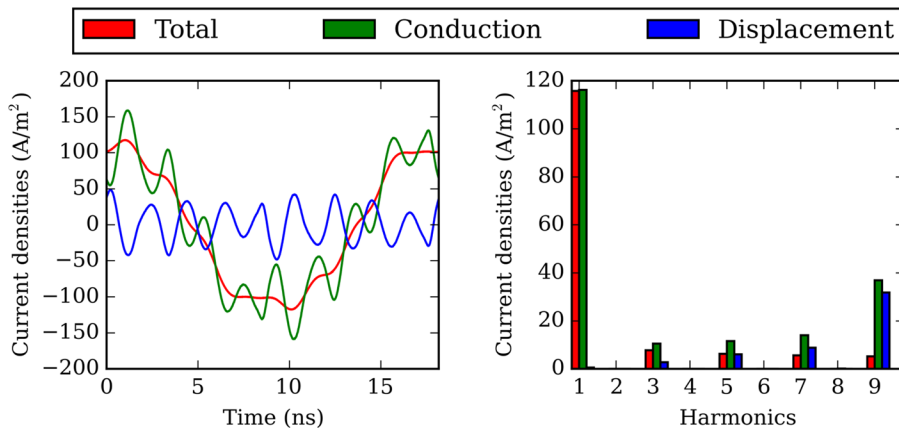
FIG. 9. Conduction, displacement, and total current density as a function of time within one RF period (left) and their corresponding Fourier spectra (right) in the center of the discharge at 7.5 mm. Discharge conditions: argon, 1.5 Pa, $L = 1.5$ cm, $f_{RF} = 55$ MHz, $\phi_0 = 300$ V.

energetic electron beam). Consequently, the number of electron beams generated during one expansion phase increases. Since the bulk electrons are now modulated by a frequency nine times higher than the applied radio frequency (nine maxima in Fig. 8(b)), a pronounced excitation of the ninth harmonic is observed in the discharge center (at $x = 7.5$ mm) in the corresponding Fourier spectra shown in Fig. 9 (right). Due to the increasing number of electron beams per sheath expansion phase, the number of extrema in the conduction and displacement current density also increases (cf. Fig. 9 left) according to the kinetic phenomena discussed in Secs. I–III.

IV. CONCLUSION

By analyzing the spatio-temporal electron dynamics based on kinetic PIC/MCC simulations of a symmetric single frequency argon CCRF plasma operated at low pressure, we explained the kinetic origin of resonance phenomena observed in terms of high frequency oscillations of the conduction, displacement, and total current waveforms in such plasmas. In this way, we linked kinetic simulations to fluid models, where such high frequency current oscillations were observed before, but where several important fundamental questions remained unanswered. In particular, we have addressed the questions: How is current continuity ensured in the presence of energetic electron beams generated by the expanding sheaths that lead to a local enhancement of the conduction current propagating through the bulk? How do the beam electrons interact with cold bulk electrons and how do they affect the EVDF? What is the kinetic origin of the observed resonance phenomena?

By splitting the total electron population into different groups according to their kinetic energies and directions of propagation in the axial direction, we showed that energetic beam electrons interact with "cold" bulk electrons (modulated at the local electron plasma frequency) via a time dependent electric field outside the sheaths. This electric field is caused by the electron beam itself, by leaving behind a positive space charge, that attracts cold bulk electrons towards the expanding sheath. This leads to the local generation of a time dependent displacement current that ensures current continuity by locally compensating the enhancement

of the conduction current. The backflow of cold electrons towards the expanding sheath, while the energetic beam electrons propagate into the opposite direction, is the kinetic mechanisms that cannot be described by fluid models based on a mean electron fluid velocity. This backflow of cold electrons causes the generation of another energetic electron beam, when these electrons hit the expanding sheath. This process is repeated until the adjacent sheath stops expanding. In this way, multiple electron beams are generated during one phase of sheath expansion. Their number depends on the response-time of the bulk electrons, which in turn is determined by their local plasma frequency. An increase of the plasma density by increasing the driving voltage amplitude, therefore, increases the number of electron beams per sheath expansion phase, as well as the frequency of the harmonics observed in the local conduction, displacement, and total current waveforms.

CCRF discharges are very complex devices and certainly other effects can also play important roles under other conditions but these kinetic mechanisms are present in any low pressure CCRF discharge (symmetric or asymmetric) and their understanding is fundamentally important for the generation of such plasmas. Although these effects are included in previous kinetic simulations of capacitive RF plasmas, their identification and understanding required the advanced diagnostics applied here (i.e., splitting the electron population into different groups and performing a detailed spatio-temporal analysis of their respective dynamics). The experimental identification of the generation of multiple electron beams per sheath expansion phase is difficult due to the required high temporal resolution (on a sub-nanosecond timescale). Therefore, in a variety of experimental studies, a single electron beam generated per sheath expansion phase is observed, which in fact, might be the result of a temporal average over multiple beams. The physical picture revealed here is significantly different from assumptions made in a variety of previous models, which assume the generation of a single electron beam. Moreover, our kinetic interpretation analysis shows that resonance phenomena, such as the plasma series and parallel resonances, might be described adequately, but cannot be fully understood in the frame of global models, since kinetic local phenomena are crucially important.

ACKNOWLEDGMENTS

[1]M. A. Lieberman and A. J. Lichtenberg, *Principles of Plasma Discharges and Materials Processing*, 2nd ed. (Wiley, New York, 2005).

[2]P. Chabert and N. Braithwaite, *Physics of Radio-Frequency Plasmas* (Cambridge University Press, 2011).

[3]S. Bienholz, N. Bibinov, and P. Awakowicz, J. Phys. D: Appl. Phys. **46**, 084010 (2013).

[4]S. Samukawa, M. Hori, S. Rauf, K. Tachibana, P. Bruggeman, G. Kroesen, J. Whitehead, A. Murphy, A. Gutsol, S. Starikovskaia, U. Kortshagen, J. P. Boeuf, T. Sommerer, M. Kushner, U. Czarnetzki, and N. Mason, J. Phys. D: Appl. Phys. **45**, 253001 (2012).

[5]P. Belenguer and J. P. Boeuf, Phys. Rev. A **41**, 4447 (1990).

[6]D. Vender and R. W. Boswell, J. Vac. Sci. Technol., A **10**(4), 1331 (1992).

[7]M. M. Turner and M. B. Hopkins, Phys. Rev. Lett. **69**(24), 3511 (1992).

[8]J. Schulze, Z. Donkó, B. G. Heil, D. Luggenhölscher, T. Mussenbrock, R. P. Brinkmann, and U. Czarnetzki, J. Phys. D: Appl. Phys. **41**, 105214 (2008).

[9]U. Czarnetzki, D. Luggenhölscher, and H. F. Dobele, Plasma Sources Sci. Technol. **8**, 230 (1999).

[10]M. A. Lieberman and V. A. Godyak, IEEE Trans. Plasma Sci. **26**(3), 955 (1998).

[11]M. A. Lieberman, IEEE Trans. Plasma Sci. **16**(6), 638 (1988).

[12]M. Surendra and D. B. Graves, Phys. Rev. Lett. **66**, 1469 (1991).

[13]M. M. Turner, Phys. Rev. Lett. **75**, 1312 (1995).

[14]G. Gozadinos, M. M. Turner, and D. Vender, Phys. Rev. Lett. **87**, 135004 (2001).

[15]M. M. Turner, J. Phys. D: Appl. Phys. **42**, 194008 (2008).

[16]I. D. Kaganovich, Phys. Rev. Lett. **89**, 265006 (2002).

[17]I. D. Kaganovich, O. V. Polomarov, and C. E. Theodosioue, IEEE Trans. Plasma Sci. **34**(3), 696 (2006).

[18]T. Lafleur, P. Chabert, and J. P. Booth, Plasma Sources Sci. Technol. **23**, 035010 (2014).

[19]T. Lafleur, P. Chabert, M. M. Turner, and J. P. Booth, Plasma Sources Sci. Technol. **23**, 015016 (2014).

[20]S. Sharma and M. M. Turner, Phys. Plasmas **20**, 073507 (2013).

[21]B. P. Wood, Ph.D. thesis, University of Berkeley, California, 1991.

[22]J. Schulze, B. G. Heil, D. Luggenhölscher, U. Czarnetzki, and R. P. Brinkmann, J. Phys. D: Appl. Phys. **41**, 042003 (2008).

[23]J. Schulze, B. G. Heil, D. Luggenhölscher, R. P. Brinkmann, and U. Czarnetzki, J. Phys. D: Appl. Phys. **41**, 195212 (2008).

[24]J. Schulze, T. Kampschulte, D. Luggenhölscher, and U. Czarnetzki, J. Phys.: Conf. Ser. **86**, 012010 (2007).

[25]J. Schulze, Z. Donkó, A. Derzsi, I. Korolov, and E. Schuengel, Plasma Sources Sci. Technol. **24**, 015019 (2014).

[26]Y. X. Liu, Q. Z. Zhang, W. Jiang, L. J. Hou, X. Z. Jiang, W. Q. Lu, and Y. N. Wang, Phys. Rev. Lett. **107**, 055002 (2011).

[27]Y. X. Liu, Q. Z. Zhang, W. Jiang, W. Q. Lu, and Y. N. Wang, Plasma Sources Sci. Technol. **21**, 035010 (2012).

[28]T. Mussenbrock and R. B. Brinkmann, Appl. Phys. Lett. **88**, 151503 (2006).

[29]T. Mussenbrock, R. B. Brinkmann, M. A. Lieberman, A. J. Lichtenberg, and E. Kawamura, Phys. Rev. Lett. **101**, 085004 (2008).

[30]U. Czarnetzki, T. Mussenbrock, and R. P. Brinkmann, Phys. Plasmas **13**, 123503 (2006).

[31]T. Mussenbrock and R. B. Brinkmann, Plasma Sources Sci. Technol. **16**, 377–385 (2007).

[32]B. M. Annaratone, V. K. T. Ku, and J. E. Allen, J. Appl. Phys. **77**, 5455 (1995).

[33]V. K. T. Ku, B. M. Annaratone, and J. E. Allen, J. Appl. Phys. **84**, 6536 (1998).

[34]V. K. T. Ku, B. M. Annaratone, and J. E. Allen, J. Appl. Phys. **84**, 6546 (1998).

[35]M. A. Lieberman, A. J. Lichtenberg, E. Kawamura, T. Mussenbrock, and R. B. Brinkmann, Phys. Plasmas **15**, 063505 (2008).

[36]Z. Donkó, J. Schulze, U. Czarnetzki, and D. Luggenhölscher, Appl. Phys. Lett. **94**, 131501 (2009).

[37]E. Schungel, S. Brandt, Z. Donkó, I. Korolov, A. Derzsi, and J. Schulze, Plasma Sources Sci. Technol. **24**, 044009 (2015).

[38]E. Schuengel, S. Brandt, I. Korolov, A. Derzsi, Z. Donkó, and J. Schulze, Phys. Plasmas **22**, 043512 (2015).

[39]B. Bora, H. Bhuyan, M. Favre, E. Wyndham, and H. Chuaqui, Appl. Phys. Lett. **100**, 094103 (2012).

[40]B. Bora, Plasma Sources Sci. Technol. **24**, 054002 (2015).

[41]M. Klick, W. Rehak, and M. Kammeyer, Jpn. J. App. Phys., Part 1 **36**, 4625 (1997).

[42]E. Semmler, P. Awakowicz, and A. von Keudell, Plasma Sources Sci. Technol. **16**, 839 (2007).

[43]B. Bora, H. Bhuyan, M. Favre, E. Wyndham, H. Chuaqui, and M. Kakati, Phys. Plasmas **18**, 103509 (2011).

[44]D. O'Connell, T. Gans, D. Vender, U. Czarnetzki, and R. Boswell, Phys. Plasmas **14**, 034505 (2007).

[45]D. O'Connell, T. Gans, A. Meige, P. Awakowicz, and R. Boswell, IEEE Trans. Plasma Sci. **36**(4), 1382–1383 (2008).

[46]C. K. Birdsall, IEEE Trans. Plasma Sci. **19**, 65 (1991).

[47]Z. Donko, Plasma Sources Sci. Technol. **20**, 024001 (2011).

[48]M. M. Turner, A. Derzsi, Z. Donkó, D. Eremin, S. J. Kelly, T. Lafleur, and T. Mussenbrock, Phys. Plasmas **20**, 013507 (2013).

[49]A. V. Phelps, J. Appl. Phys. **76**, 747 (1994).

[50]A. V. Phelps, see http://jilawww.colorado.edu/~avp/collision_data/ for cross sections for the simulation.

[51]S. Wilczek, J. Trieschmann, J. Schulze, E. Schuengel, R. P. Brinkmann, A. Derzsi, I. Korolov, Z. Donkó, and T. Mussenbrock, Plasma Sources Sci. Technol. **24**, 024002 (2015).

[52]M. Klick, J. Appl. Phys. **79**, 3445 (1996).